SP2016_3124991

INVESTIGATION OF PRESSURE HAMMER WITH WIRE MESH SENSOR AND HIGH SPEED IMAGING TECHNIQUES

Tobias Traudt[1] [*], Cristiano Bombardieri[1], Eckhard Schleicher[2], Chiara Manfletti[1]

[1] Institute of Space Propulsion, German Aerospace Center (DLR), Langer Grund, 74239 Hardthausen (Germany), Email: tobias.traudt@dlr.de
[2] Institute of Fluid Dynamics, Helmholtz-Zentrum Dresden-Rossendorf e.V. (HZDR), Bautzner Landstrasse 400, 01328 Dresden (Germany), Email: e.schleicher@hzdr.de

KEYWORDS: water hammer, pressure hammer, cavitation, high speed imaging, wire mesh sensor

ABSTRACT

Previous water hammer tests have revealed pressure spikes in the cavitation regime. With the aim of explaining the phenomena and enhancing the understanding of the pressure hammer phenomenon in general, a high speed imaging (HSI) setup was installed at the test bench. To complement the high speed imaging a wire mesh sensor was used. The wire mesh sensor (WMS) allowed the measurement of the cross-sectional void fracture distribution in the pipe while the flow was cavitating. The results of the measurements are presented and discussed.

1. INTRODUCTION

Water hammer is of strong interest in many industrial fields, amongst which the space industry. In rocket engines and thrusters it plays a major role in

Water hammer is a well-studied phenomenon because of its importance for designers of fluid systems. For CFD tools it provides for a valuable validation, to check whether the code is able to correctly simulate steep pressure gradients, absolute pressure peaks and wave attenuation. When the pressure falls below the saturation pressure and hence column separation occurs, the complexity of flow simulation increases significantly because of instantaneous evaporation and condensation.

In order to investigate these phenomena at pressures of up to 100 bar and Reynolds numbers of up to 10^5 a test bench was built at the DLR Lampoldshausen. Tests were performed with water to produce a pressure surge upon valve closing.

In the next sections the test bench setup and the experimental method will be presented. We will show the reproducibility of the experiments and subsequently present the experimental findings.

As the focus was on cavitation, a wire mesh sensor was installed to measure void fraction and to support numerical simulations with quantitative measurements.
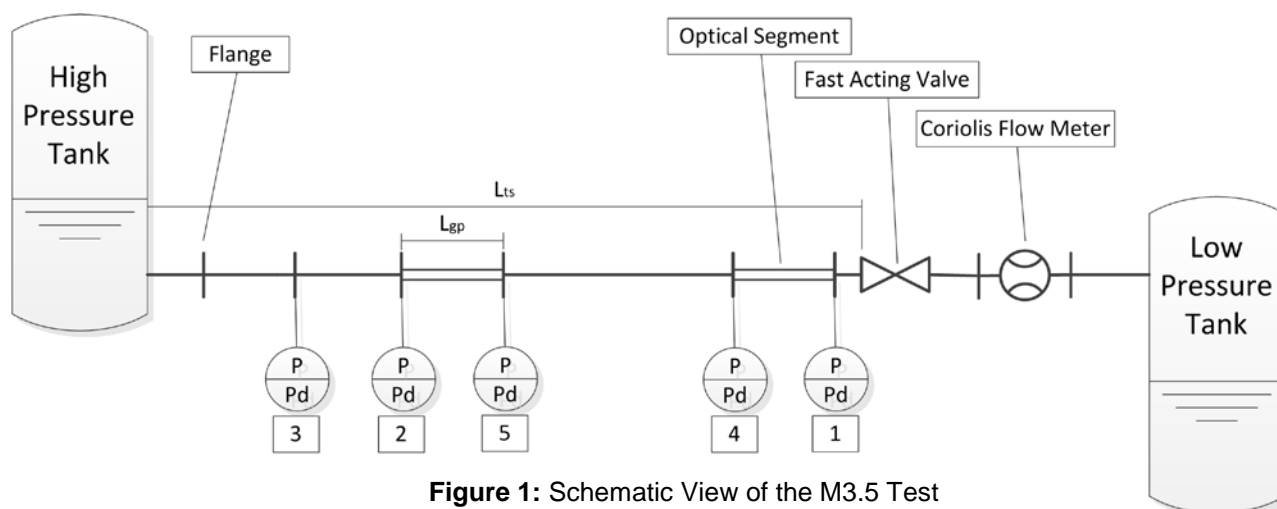
Additionally optical access to the test section

Figure 1: Schematic View of the M3.5 Test Bench.

the designing process of the feed system and has to be considered especially when the feed lines are primed during start-up as well as during the rapid closing of valves upon shutdown. In both cases a pressure peak will occur, leading to a water hammer wave travelling along the pipe.

proved to be an indispensable tool to understand how and where the liquid evaporates and how the vaporous regions reintegrate; hence a high speed imaging setup was installed.

We will show the results of the WMS in a pseudo 3D plot, cross sectional images and cross section

averaged values. The HSI will be presented in a series of images showing the evaporating liquid.

2. EXPERIMENTAL METHOD

Testing was conducted using the test bench M3.5. The test bench was designed to investigate pressure

Figure 2: Support structure in Configuration A and B.

hammer and priming phenomena. The main parts of the test bench are the two tanks, the pressurization system, the test section, and the fast acting valve. The fast acting valve is coaxial and is pneumatically actuated. By controlling the working pressure of the

Table 1: Dimensions in the high speed imaging setup

Description	
Test section length, L_{ts}	8.376 m
Sensor distance from valve seat, Position 1	0.3 m
Sensor distance from valve seat, Position 2	7.45 m
Sensor distance from valve seat, Position 3	8.13 m
Sensor distance from valve seat, Position 4	0.57 m
Sensor distance from valve seat, Position 5	7.18 m
Outer diameter optical segment	35 mm
Inner diameter optical segment	19 mm
Length optical segment, L_{gp}	250 mm

valve the closing time can be regulated. The closing time is recorded using the valve's position encoder. In the tests discussed in this paper, the measured valve closing time was 22 ms.

The pressurization system uses nitrogen or

helium. Setting a differential pressure between the tanks controls the initial flow speed in the test section. Automatically controlled pressure regulators and discharge valves at both tanks ensure that the pressure level is within ± 0.4 % prior to valve closing.

The test bench is equipped with a Coriolis flow

Table 2: General dimensions of test bench.

Description	
Test section inner pipe diameter, $d_{i,ts}$	19 mm
Test section wall thickness, e_{ts}	1.5 mm
Diameter of coiled test section	1.25 m

meter for mass flow measurement. For the mass flows presented in this paper, the device is precise to < 0.1 %. The flow meter is installed downstream of the fast acting valve.

The main dimensions of the test section are shown in Table 2. The longest segment of the test section is wound into a spiral with a diameter of 1.25 m. The material of the test section is stainless steel of grade 1.4541. To limit its movement, it is mounted onto a rigid support structure at seven points. The support structure is made of aluminium profiles. The test section is mounted with an upward slope of about 1°.

Table 3: Dimensions in the wire mesh sensor setup

Description	
Test section length, L_{ts}	7.876 m
Sensor distance from valve seat, Position 1	0.3 m
Sensor distance from valve seat, Position 2	6.94 m
Sensor distance from valve seat, Position 3	7.64 m
Wire Mesh Sensor, distance measurement plane to valve seat	0.32 m

The segments of the test section are connected by flanges. In between the flanges, 20 mm long disks, with the same inner diameter as the test section, are installed in which three sensors are mounted. Each disk houses one type K thermocouple, one piezo-resistive static pressure sensor (Kistler 4043-A100 type) and one piezo-electric dynamic pressure sensor (Kistler 601A). The static pressure sensors and the dynamic pressure sensors are flush mounted. The sampling rate for the static pressure sensors is set to 10 kHz and for the dynamic pressure sensors it is set to 150 kHz. To avoid aliasing, Butterworth filters in the amplifiers are set to 2 kHz and 30 kHz (-3 dB) respectively.

Three sensor disks are installed at positions upstream of the fast acting valve. The distance of each set of sensors to the valve seat of the fast acting valve is listed in Table 2.

The upstream tank has a flanged connection with

an inner diameter of 98.3 mm (DN100). The inlet from the side facing flange to the test section has rounded edges with a radius of 5 mm. The length of the DN100 segment inside the tank is 218 mm.

The maximum Reynolds numbers for the initial conditions prior to valve closing, which have been demonstrated to the present day, are *Re* = 68000 for water hammer experiments without cavitation and *Re* = 118000 for tests with cavitation.

High Speed Imaging Setup

Two optical segments made of quartz glass were installed in the test section for optical access (see Figure 3). They were not used simultaneously to the wire mesh sensor.

One optical segment is located next to the fast acting valve, while the other is close to the high pressure tank (see Figure 1). Both were of the same type (see Table 1). The one close to the valve was used for image recording, while the other one was not used.

Figure 3: Optical Segment.

A Photron Fastcam SA-X was used for image acquisition. The following settings were used for all videos presented in this paper:

- Frame rate: 19,200 fps
- Shutter: 1/22222 s
- Resolution: 1024 x 200 pixels;
                   0.23 mm/pixel

The backlight was provided by a flashlight of type LedLenser X21 in conjunction with an optical diffusor. Both were placed in the line of sight of the camera behind the quartz glass segment.

Wire Mesh Sensor (WMS)

Wire mesh sensors are well-known tools for visualization and quantification for two-phase pipe flows. Introduced in 1998 by Prasser et al. [1], the technique has widely spread in fluid dynamic investigations for conducting experimental investigation of interfacial structures [2] as well as non-conducting liquids [3]. A wire mesh sensor consists of two planes, the transmitter and the receiver plane, of parallel wires stretched equidistantly across a pipe or vessel cross section. The wires in the transmitter plane are arranged perpendicular to those

of the receiver plane and positioned with a small axial gap. Hence, the transmitter and receiver wires form virtual crossing points. By applying an excitation signal to the transmitter wires, one by one, and measuring the resulting signals at the receiver wires, via the corresponding electronics, the electrical properties (conductivity or capacitance) in these virtual crossing points are recorded. This scheme can be made very fast and allows frame rates up to 10,000 fps, enabling the technique to acquire sharp cross sectional images of highly transient flow situations. For this work a conductivity wire mesh sensor electronics was used. A bipolar voltage pulse of 6 µs is applied to the transmitter wires and the resulting current flowing through the medium is measured in the receivers via trans-impedance amplifiers and digitized with 12 bit ADCs.

From the acquired raw data the local instantaneous void fractions $\varepsilon(i,j,k)$ of each crossing point [i,j] for each frame number k can be calculated assuming a linear relation between the local gas holdup and the current flowing from the transmitter towards the receiver wires. This can be expressed by $\varepsilon(i,j,k) = 1 - ADC_{mess}(i,j,k)/ADC_{water}(i,j)$ with the local instantaneous readings $ADC_{mess}(i,j,k)$ and the full water calibration values $ADC_{water}(i,j)$ which are usually taken by averaging over a certain period with the complete liquid filled sensor. From the resulting void fraction data, secondary physical parameters such as cross sectional averaged void fractions over the time, temporal averaged cross sectional or radial void fraction distributions can be derived. Stacking the data frame wise, allows deriving, in addition to cross sectional movies, also pseudo three-dimensional visualizations and pseudo side cuts for a better visual impression of the flow behaviour.

The wire mesh sensor utilized in this study is built of stainless steel wires with 200 µm in diameter. The 8 x 8 wire grid leads to a resolution of 2.2 mm.

The grid size is a trade-off between minimizing the influence of the sensor on the flow on the one hand and maximizing the resolution on the other hand. The influence on the flow has to be kept to a minimum in pressure hammer experiments because when the flow is cavitating the water is at its saturation point and each additional pressure drop might cause vapour bubbles to form, distorting the measurement.

The sensor was installed next to the pressure sensor in position 1 (see Figure 1).

Acoustics

The speed of sound in the test section was measured to be $c_f = 1345$ m/s (for a discussion of the method implemented refer to [4]).

The periods of a pressure wave travelling from the fast acting valve to the upstream tank and back to valve are $T_f = 2 \cdot L/c_f = 12.4$ ms for the high speed imaging setup (HSI) and 11.7 ms for the WMS setup. The effective valve closing time $T_{c,eff} = 0.3 \cdot T_c = 6.6$ ms $< T_f$ is thus low enough to yield the maximum

expected water hammer peak pressure which is the Joukowski pressure [5].

Test Procedure and Reproducibility

Before each test day the upstream tank is filled with water and the test section is purged to remove any entrapped air. This is necessary for several reasons. Air in the test section lowers the speed of sound, it cushions the column reintegration after a cavitation event and bubbles of air in the flow will act as nucleation sites during cavitation. Due to the latter, instantaneous evaporation might happen at locations different to the case in which there are no bubbles of noncondensable gas in the flow.

The water in the test bench is stored overnight at ambient pressure to ensure that there are no non-dissolved gas bubbles left in the water. For testing, the pressure in the tanks is set to the desired values, the fast acting valve is opened and the water starts to flow. Before the valve is closed the water is allowed to flow for a few seconds in order to establish stationary flow. After each test, gas which might have dissolved come out of the liquid, is vented from the valve seat of the fast acting valve using opening a dedicated purging valve.

The tests are repeated at least three times to examine the reproducibility of the results. Good reproducibility was achieved for all tests presented in this paper. As an example, Figure 4 shows the pressure evolution of the static pressure sensor at position 1.
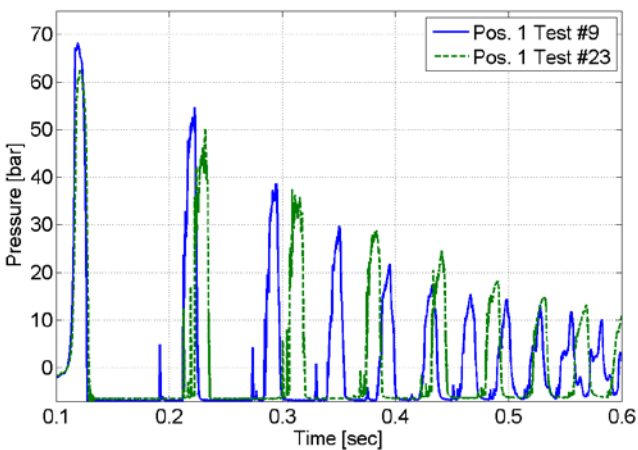

Figure 4: pressure plots of tests with wire mesh sensor (test #9) and high speed imaging setup (test #23).

An image of the cavitation inside the pipe is added to show that although the reproducibility of the pressure evolution is very good, the reproducibility of the positions of the cavitating bubbles are not. This is due to nucleation sites. It is well known (Naterer [6]) that vapour bubbles form when there is a nucleation

site. Nucleation sites maybe microscopic roughness at the wall, as well as microscopic bubbles of undissolved air or dirt particles. Since nucleation sites are distributed randomly over the pipe cross section it is not foreseeable where a bubble will start to form. As a side effect the local void distribution of one test will
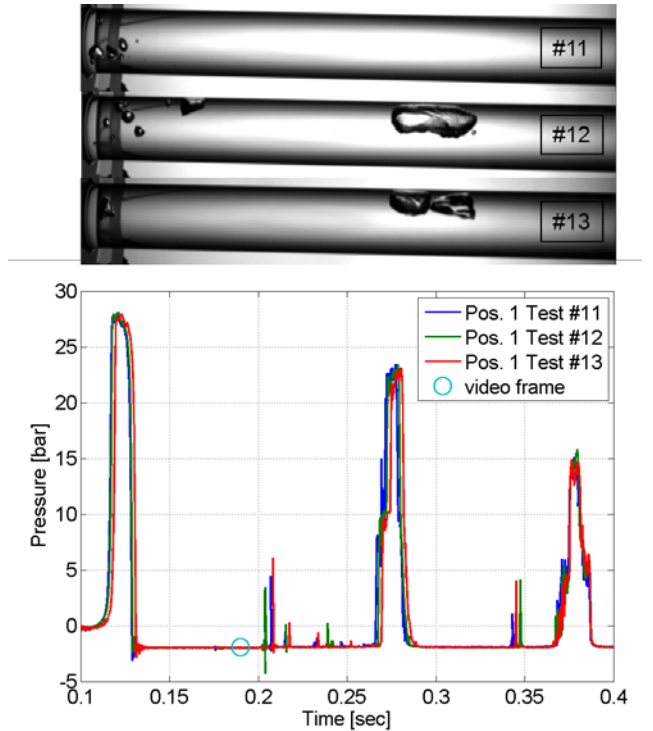

Figure 5: video frames of three tests at the same time (top), position of the frames in pressure plot (bottom).

be totally different to another (see Figure 4). This is true although the pressure plots show a good repeatability for consecutive tests. The latter leads to the conclusion, that the global void fraction in the entire pipe is comparable.

The test condition for these tests and all the following tests are summarized in Table 4.

Table 4: Test Settings Pressure Hammer

Test #	Mean tank pressure (bar)	Initial flow velocity (m/s)	Setup
9	7	5.15	WMS
11	1.5	2.06	HSI
12	1.5	2.08	HSI
13	1.5	2.06	HSI
23	6	4.73	HSI

3. RESULTS AND DISCUSSION

Figure 4 depicts pressure plots for test #9 with the WMS setup and test #23 with the HSI setup.

The high speed imaging setup (HSI) was not used in the same tests as WMS. However, the plots show that there is a difference in the height of the first pressure peak of 7.6 % and the cavitation period in
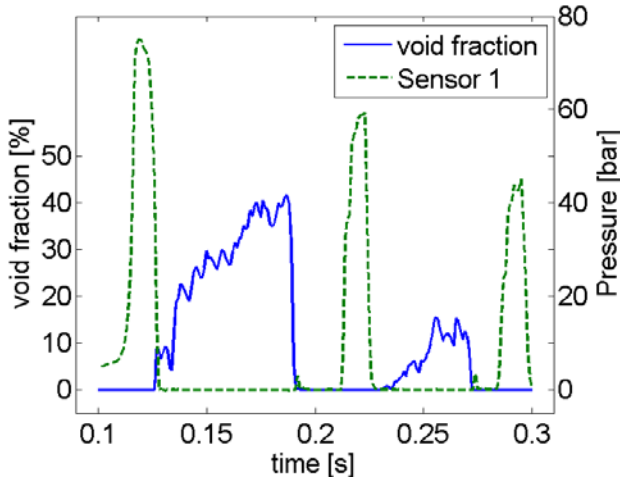

Figure 6: pressure plots versus cross section averaged void fraction.

the HSI setup is 10% longer due to the longer test section and the difference in initial flow velocity.

Tests #9 and #23 were chosen because the cavitation period (time between two pressure peaks) is long in comparison to the duration of the water hammer pressure peaks period (see Figure 7). The longer the cavitation period the more vapour will form in the pipe which helps in the visualization and measurement of the voids.

An interesting phenomenon in both tests is the short duration pressure spikes in the cavitation area (arrow in Figure 7). This phenomenon was observed in experiments by Bergant, et.al. [7] and it was speculated to be a pressure sensor artefact. However as presented in a past publication we were able to visualize the spikes in the HSI tests [8].

To complement the HSI and to enhance the understanding of this phenomenon as well as the pressure hammer in general the WMS was added to the test section.

Figure 8 shows the void fraction recorded by the WMS over the cross section. At the top of the image is a pseudo 3D rendering of the void fraction distribution. In the graph the time is used as a third dimension to render a 3D volume.

The pseudo 3D vapour cavity on the left side in Figure 8 represents the vapour evolution in the first cavitation period (0.18 s to 0.21 s). Its shape is comparable to
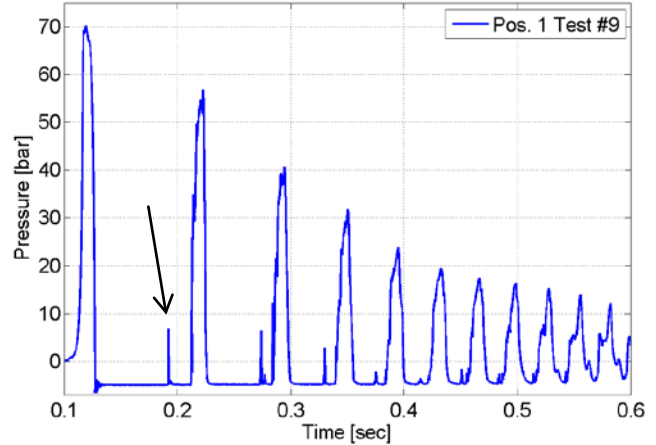

Figure 7: Pressure plot of test with wire mesh sensor; the arrow indicates a short duration pressure spike.

the bubble entering the glass segment from the left side in Figure 10(1).

The data from the pseudo 3D view is plotted as the cross section averaged void fraction in Figure 8 (bottom). It shows that vapour bubbles can fill up to 40 % of the pipe volume. The resolution of the sensor – although very low with only 8x8 pixel – is enough to recover void fraction distributions over the cross section. However, there are limitations. After about 0.19 seconds there is no void measured by the WMS. Looking at Figure 10(10) it becomes clear that this is due to the short pressure spike in the cavitation area after which there are only very small bubbles left. These bubbles are not detectable by the WMS. As mentioned before the tests are slightly different due to the different test section lengths and setups (see section 2).
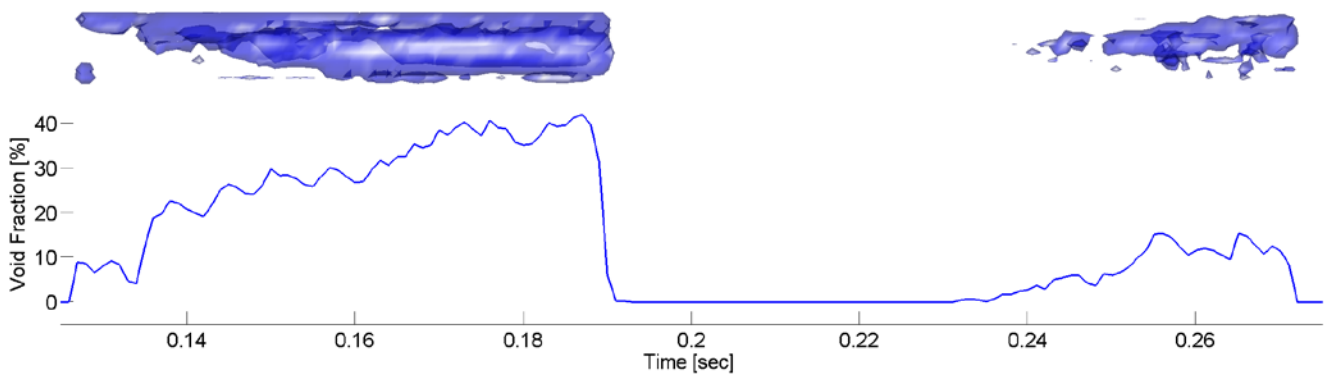

Figure 8: pseudo 3D view of void fraction (top); cross section averaged void fraction (bottom).
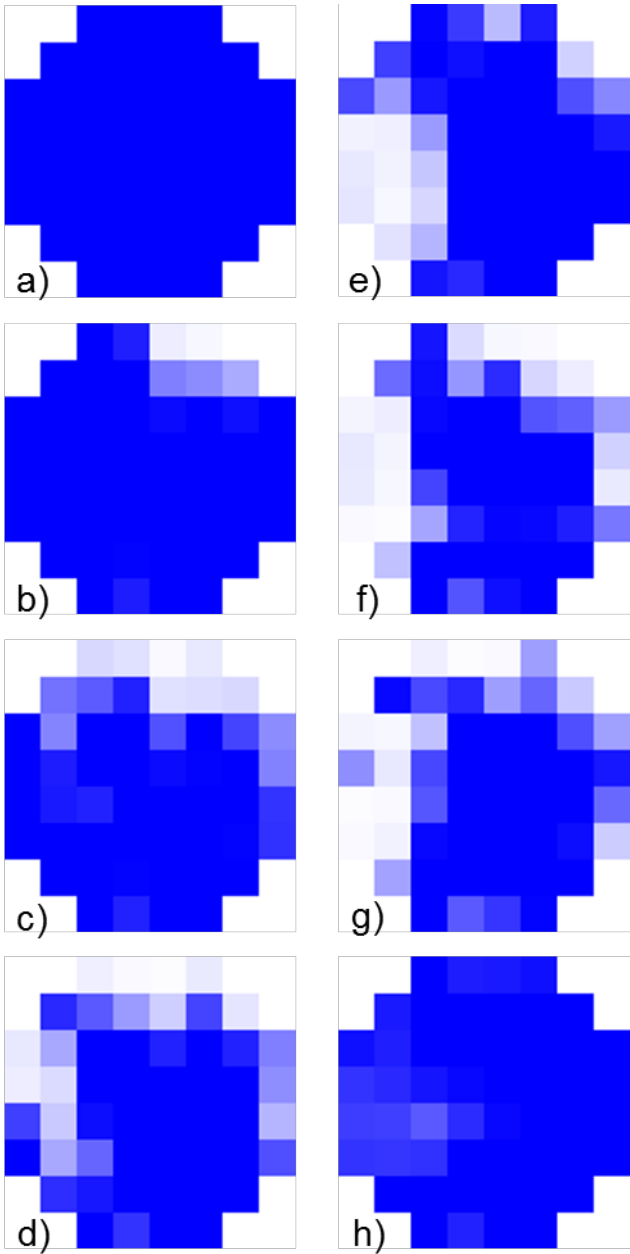
Figure 9: void fraction distribution at position 1; the frames are equally spaced by 10 ms (top); position of void measurements (bottom).
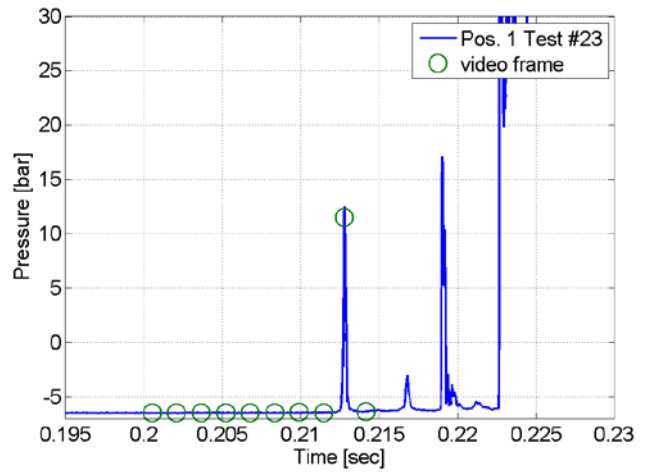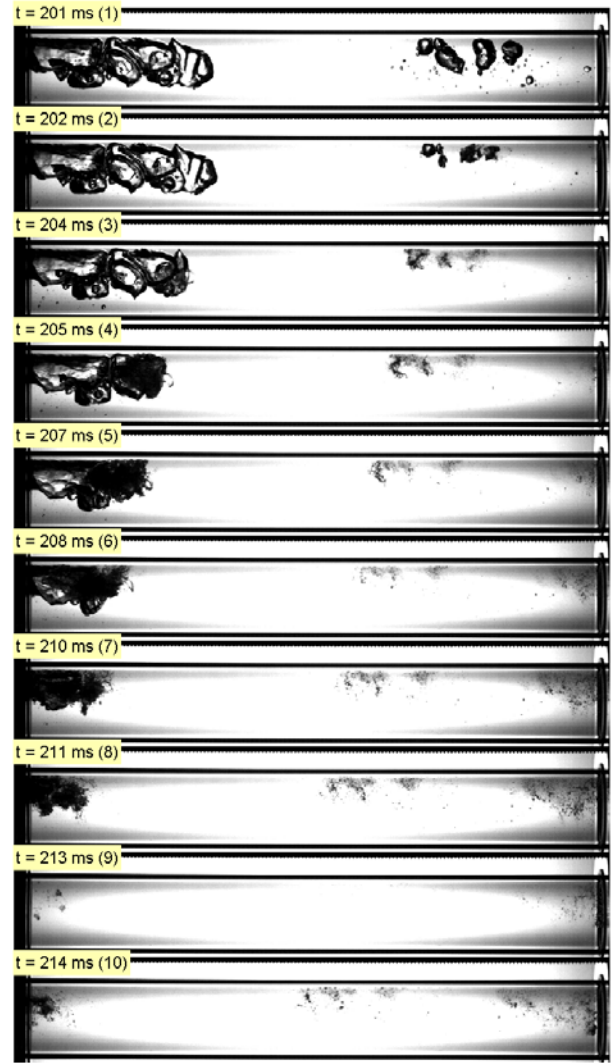
Figure 10: video frames of test #23 (top); position of video frames (bottom).

Another visualisation of the void fraction measurements by the WMS can be found in Figure 9. Here the distribution over the cross section is shown. The time between the images is 10 ms.

The pictures show a cavity which starts forming at

the top right of the pipe. After 40 ms (d) a second cavity starts to form at the left side of the pipe. Both cavities keep evolving until the short duration spike is measured in the pressure plot (h, Figure 9).

In the aforementioned publication [8] the authors had postulated that these short duration spikes were related to the reversal of the flow.

Flow reversal is inherent to the pressure hammer experiment with cavitation. In pressure hammer experiments the flow in the line is stopped by the valve. As a consequence the pressure rises in front of the valve and travels upstream towards to upstream tank. The pressure wave is then reflected at the upstream tank, travels towards the valve and reflects at the valve as an expansion wave. When the pressure drops below the saturation pressure, the liquid will start to cavitate. The liquid/vapour mixture will now flow away from the valve until the kinetic energy is zero. At this point the liquid/vapour mixture will reverse and flow towards the valve. The time when it impacts at the valve is the beginning of the second pressure peak.

In Figure 10 the flow reversal can easily be tracked over frames 1 to 8. The short duration spike on the other hand has its peak in frame 9. The results hence show that the observed short duration spikes do not coincide with the flow reversal. Furthermore, the duration of the flow reversal is large (in the order of 10 ms) in comparison to the short duration spike (in the order of 1 ms).

The short duration spike leads to instantaneous bubble collapse, after which there are no big bubbles anymore. The bubble size is smaller than the resolution of the WMS which is why the sensor no longer detects void volumes.

4. CONLCUSION

Quantitative two dimensional void fraction measurements during the cavitation phase of a pressure hammer event were presented and discussed.

The possibilities of the wire mesh sensor used for the measurements as well as its limitations were shown. The wire mesh sensor gives very good two dimensional void fractions results especially during the first period of the pressure hammer event. After the first column collapse the size of the vapour bubble decreases significantly, falling below the resolution of the sensor.

Tests with a high speed imaging setup complemented the measurements with the wire mesh sensor. The high speed images showed that the flow reversal during the cavitation event is not coinciding with the short pressure spikes published in literature. The cause of the short duration pressure spikes still remains unclear. Additional experiments as well as numerical work will be performed to investigate their origin.

REFERENCES

[1] H.-M. Prasser, A. Böttger und J. Zschau, „A new electrode-mesh tomograph for gas-liquid flows," *Flow Measurement and Instrumentation ,* Bd. 9, Nr. 2, pp. 111-119, 1998.

[2] M. Parsi, R. E. Vieira, C. F. Torres, N. R. Kesana, B. S. McLaury, S. A. Shirazi, E. Schleicher und U. Hampel, „Experimental investigation of interfacial structures within churn flow using a dual wire-mesh sensor," *International Journal of Multiphase Flow ,* Bd. 73, pp. 155-170, 2015.

[3] M. J. Da Silva, E. Schleicher und U. Hampel, „Capacitance wire-mesh sensor for fast measurement of phase fraction distributions," *Measurement Science and Technology,* Bd. 18, Nr. 7, p. 2245, 2007.

[4] T. Traudt, C. Bombardieri und C. Manfletti, „Influences on Water Hammer Wave Shape an Experimental Study," in *63. Deutscher Luft- und Raumfahrtkongress, Augsburg Germany*, 2014.

[5] A. S. Tijsseling, „Poisson-Coupling Beat in Extended Waterhammer Theory," *ASME,* Bd. 53, pp. 529-532, 1997.

[6] Naterer, G., Heat Transfer in Single and Multiphase Systems, *CRC Press,* **2002**

[7] A. Bergant und A. Simpson, „Pipeline Column Separation Flow Regimes," *Journal of Hydraulic Engineering,* 1999.

[8] T. Traudt, C. Bombardieri und C. Manfletti, „High Speed Imaging of Water Hammer with Column Separation," in *Pressure Surge Conference, Dublin*, 2015.